Effect of ionic radius and valence state of alkali and alkaline earth metals on promoting the catalytic performance of La_2O_3 catalysts for glycerol carbonate production

Yu, Jialin; Wang, Ke; Shao, Shibo; Li, Wei; Du, Shangfeng; Chen, Xianfeng; Chao, Cong; Fan, Xianfeng

DOI:
10.1016/j.cej.2023.141486

Document Version
Publisher's PDF, also known as Version of record

Citation for published version (Harvard):
Yu, J, Wang, K, Shao, S, Li, W, Du, S, Chen, X, Chao, C & Fan, X 2023, 'Effect of ionic radius and valence state of alkali and alkaline earth metals on promoting the catalytic performance of La_2O_3 catalysts for glycerol carbonate production', *Chemical Engineering Journal*, vol. 458, 141486.
https://doi.org/10.1016/j.cej.2023.141486

Chemical Engineering Journal 458 (2023) 141486

Contents lists available at ScienceDirect

Chemical Engineering Journal

journal homepage: www.elsevier.com/locate/cej

Effect of ionic radius and valence state of alkali and alkaline earth metals on promoting the catalytic performance of La_2O_3 catalysts for glycerol carbonate production

Jialin Yu [a], Ke Wang [a], Shibo Shao [a], Wei Li [a], Shangfeng Du [b], Xianfeng Chen [a], Cong Chao [c,*], Xianfeng Fan [a,*]

[a] School of Engineering, The University of Edinburgh, Edinburgh EH9 3FB, UK
[b] School of Chemical Engineering, University of Birmingham, Birmingham B15 2TT, UK
[c] Beijing Key Laboratory of Construction Tailorable Advanced Functional Materials and Green Applications, School of Material Science & Engineering, Beijing Institute of Technology, Beijing 100081, China

ARTICLE INFO

Keywords:
Alkali metal
La_2O_3
Ionic radius
Catalysis
Glycerol, glycerol carbonate

ABSTRACT

Alkali metals and alkaline earth metals have been used to promote the catalytic performance of metal oxides in transesterification of glycerol and dimethyl carbonate, however, the promotional roles of the dopants in influencing the catalytic performance of the metal oxides have not been fully investigated which hinder the development of low-cost and high-efficiency catalysts in transesterification of glycerol and dimethyl carbonate. This paper, for the first time, systematically studied the influence of ionic radius and valence state of dopants, surface concentration of dopants and the basicity of the catalysts on the catalytic performance of La_2O_3 in transesterification of glycerol and dimethyl carbonate. Our results suggest that the ionic radius and valence state of the dopants are the determining factors, while the basic site density is not a crucial factor, although the basicity of catalyst surface is important in activating glycerol and dimethyl carbonate. Among alkali and alkaline earth metals, 25 mol% Na/La_2O_3 catalyst achieved the highest glycerol conversion (85 %) and glycerol carbonate yield (60 %) in the 70 °C and 2-hour reaction. After the detailed investigation, a plausible mechanism of glycerol and dimethyl carbonate transesterification on Na/La_2O_3 catalyst has been proposed. This research could help understand the promotional role of alkali metals and alkaline earth metals and the results may guide future design of metal oxide catalysts.

1. Introduction

Biodiesel is regarded as a promising transmit solution to alleviate the environmental issue of burning fossil fuels [1,2]. However, the intensive development of the biodiesel industry has resulted in a huge accumulation of glycerol, a by-product from the biodiesel production process, which has led to abundant glycerol waste and a dramatically price drop in glycerol market that is further struck the economic profit of producing biodiesel [3,4]. Thus, converting glycerol into value-added products has become a promising approach to solve the problems of glycerol waste and improve the economics of biodiesel processes [4,5]. Among the various value-added products, glycerol carbonate (GLC) with the versatile properties can provide a wide range of applications [5,6], for example using as a solvent, a cosmetic ingredient, a laundry detergent, a building eco-composite, or a chemical intermediate [5–7]. Therefore, the value-added conversion of GL to GLC has attracted wide attentions, and four main methods have been developed to convert GL into GLC: (1) carbonization with phosgene or carbon monoxide [6]; (2) direct reaction with CO_2 [8]; (3) glycolysis with urea [9]; and (4) transesterification with dimethyl carbonate (DMC) [7,10,11]. Comparing the pros and cons of each of these four methods — such as the toxicity of co-reactant, thermodynamic equilibrium limitation of the reaction, difficulties in by-product separation, and the reaction conditions — GL conversion with DMC (shown in Scheme 1) appears to be the most promising route to form GLC, as DMC has been considered as a green chemical and this conversion route can be conducted at relatively mild operational conditions.

Converting GL with DMC to GLC requires the presence of catalysts,

* Corresponding authors.
E-mail addresses: 7520210001@bit.edu.cn (C. Chao), X.Fan@ed.ac.uk (X. Fan).

https://doi.org/10.1016/j.cej.2023.141486
Received 10 November 2022; Received in revised form 4 January 2023; Accepted 15 January 2023
Available online 18 January 2023

where homogenous catalysts, such as KOH, NaOH, and H_2SO_4, have been reported to achieve excellent catalytic performance, but this type of catalyst is difficult to separate from the reaction system [12]. Thus, heterogeneous catalysts have attracted more attention due to their efficient recyclability and good catalytic performance. Compared to acid catalysts, the presence of base catalysts can lead to relatively high yield and selectivity of glycerol carbonate, and also fast reaction rate in the transesterification of GL and DMC [12], which has been reported that the basic site of a catalyst is responsible for activating GL by cleaving its O—H bonds [13,14]. Liu et al. [15] established a good correlation between catalytic activity and surface basicity for transition metal doped hydrotalcite catalysts. However, it is still debatable if tuning the amount and strength of catalyst basic sites can determine their catalytic performance in GL transesterification. For example, Hu et al. [16] reported that 15 wt% K/CaO catalyst calcinated at 700 °C shows higher glycerol conversion (99 %) than CaO (92 %) in the transesterification of GL and DMC, but the amount of basic sites of 15 % K/CaO-700 (30.37 mmol/g) is lower than that of CaO (33.93 mmol/g). MgO with a trapezoidal morphology has been synthesized and tested in glycerol transesterification, and it showed the highest glycerol conversion and GLC yield but with the lowest amount and weakest strength of basic sites compared to the MgO catalyst in a rod-like, spherical, flower-like, and nest-like structure [17]. Therefore, the surface basicity of a catalyst might not be the only factor that affects its catalytic performance in the glycerol transesterification.

In addition, alkali and alkaline earth metals are high abundant in Earth's crust [18], in particular calcium, sodium, magnesium and potassium, and their unit price is relatively cheap which provides great potential to be applied in industry. So, many alkali and alkaline earth metal based and modified catalysts have been studied in transesterification of GL and DMC, for example, introducing lithium to ZnO, La_2O_3 and ZrO_2 support catalyst have been found significantly enhanced the conversion of glycerol to GLC from barely converted to over 90 % [7,19,20]. Moreover, the ionic radius and valence state of the alkali and alkali metals have been reported playing important roles on the doping location and coordination sphere, which further influence their catalytic abilities. Sugiura et al. [21] studied the alkali metal ion substitution on a layered calcium phosphate compound (octacalcium phosphate), and revealed that the difference in ionic radius between alkali metal and calcium affects the location of alkali metal ions in the layered compound. Ferreira et al. [22] used diffuse reflectance UV–vis spectra to analyse the coordination number changes of CeO_2 after the addition of Ca and Mg, with Ca/CeO_2 showing a lower coordination number (approximately 8) of Ce^{4+} ions. However, the effect of alkali and alkaline earth metals in improving the catalytic performance of metal oxides for glycerol carbonate production has not been fully understood. Additionally, no systematic investigation into the different combinations of the modifiers and base metal oxides currently exists, which has hindered the development of effective catalysts and efficient catalytic processes in glycerol value-added conversion.

Therefore, this research work presents a systematically study of the promotional roles of alkali and alkaline earth metals on improving catalytic performance of La_2O_3 in transesterification of GL and DMC. The ionic radius and valence state for alkali and alkaline earth metals were found as dominant factors for improving the catalytic activity of La_2O_3, and other factors including molecular weight, surface composition, crystallinity, electron status, specific surface area and basicity of modified La_2O_3 samples were further elucidated.

2. Experimental and characterisation

2.1. Materials

All chemicals used in this work are of analytical grade and without further purification. Lanthanum nitrate ($La(NO_3)_3{\cdot}6H_2O$), ammonium carbonate, magnesium nitrate ($Mg(NO_3)_2$), barium nitrate ($Ba(NO_3)_2$), N,*N*-dimethylformamide (DMF, 99 %), glycerol (99 %), methanol (99 %) and tetraethylene glycol (99 %) were purchased from Alfa Aesar. Lithium nitrate ($LiNO_3$), sodium nitrate ($NaNO_3$), potassium nitrate (KNO_3), calcium nitrate ($Ca(NO_3)_2$), strontium nitrate ($Sr(NO_3)_2$), dimethyl carbonate (99 %), 4- (hydroxymethyl)-1,3-dioxolan-2-one (90 %) were purchased from Thermo Fisher Scientific Inc. Glycidol (96 %) was purchased from Sigma-Aldrich.

2.2. Catalyst preparation

The support material, La_2O_3, was synthesised using a modified version of the precipitation method from Li et al. [19]. The preparation process is as follows, 0.03 mol lanthanum nitrate and 0.12 mol ammonium carbonate were each dissolved in 120 ml deionised (DI) water. The obtained ammonium carbonate solution was slowly added into lanthanum nitrate solution under mechanical stirring at room temperature and continuously stirred for 6 hrs. Then the white precipitate was separated in a centrifuge (SIGMA® 2-16P) and washed with DI water. Finally, the solid paste was dried at 110 °C for 24 hrs and calcined at 800 °C for 6 hrs in a Muffle furnace (Carbolite® ELF 11/14B) to obtain final La_2O_3 catalysts.

La_2O_3 doped by 25 mol% alkali and alkaline earth metals were prepared by wet impregnation method. A certain amount of $M(NO_3)_n$ (where M = Li, Na, K, Mg, Ca, Sr, Ba; n = 1,2) was dissolved in DI water and then 0.5 g La_2O_3 powder was added. The suspension was magnetically stirred for 12 hrs. The resulting slurry was evaporated at 80 °C in a water bath to remove excess water. The solid residue was dried at 110 °C for 10 hrs and then calcined at various temperatures (400 °C − 800 °C) for 2 hrs.

The samples were denoted as xM/La_2O_3T, where × represents the mass percentage or molecular percentage, M represents the alkali and alkaline earth metal, and T represents the calcination temperature. The default value for × and T are 25 mol% and 600 °C when the sample presented without 'x' and/or 'T'.

2.3. Catalyst characterisation

The crystal phases of pristine and modified La_2O_3 catalysts were characterised by powder X-ray diffraction (XRD) using a Bruker Phaser-D2 diffractometer with Cu Kα X-ray source. The scanning range (2θ) was from 10° to 90°, with a slit of 1° at a scanning rate of 10° min^{-1}. The electron states for the samples were analysed via X-ray photoelectron spectroscopy (XPS), conducted on a Thermo Scientific™ K-Alpha™+ spectrometer equipped with a monochromatic Al Kα X-ray source (1486.6 eV) operating at 100 W. All peaks have been calibrated with C1s peak where the standard binding energy (B.E.) is 284.8 eV for adventitious carbon source. The basicity of the samples was tested via CO_2 temperature-programmed desorption (TPD). This was carried out by

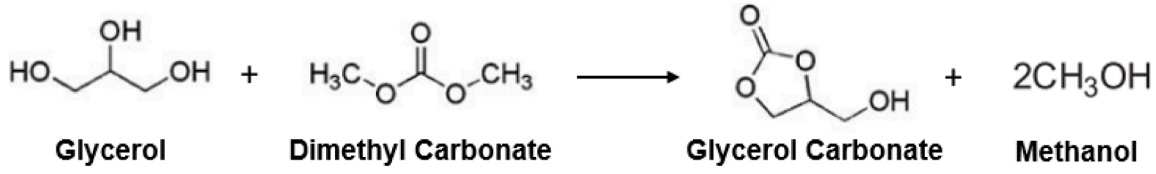

Scheme 1. Scheme of synthesis glycerol carbonate from glycerol and dimethyl carbonate.

placing a 0.10 g sample into a U-shape reactor and pre-treating it under Helium flow (at 50 sccm) at 600 °C for 30 mins. CO_2 was then introduced and adsorbed on the samples for 45 mins at room temperature. During the desorption process, the cell was heated up to 1000 °C with a ramping rate of 10 °C min^{-1} under the Helium flow (at 50 sccm).

The amount of alkali and alkaline earth metal doped on La_2O_3 was analysed by inductively coupled plasma optical emission spectrometry (ICP-OES) operated on a Varian Vista Pro instrument with axial view. The samples were digested in aqua regia and then diluted to a certain concentration before the measurements. The surface area and pore size distribution of the samples was determined via the N_2 physical adsorption–desorption experiments at 77 K in a chemisorption (& physisorption) gas sorption analyser (Quantachrome autosorb IQ). The samples were first degassed at 200 °C in vacuum for 2 hrs, and then their N_2 isotherms were measured and analysed based on the Brunauer-Emmett-Teller (BET) equation theory. The morphology of the samples was determined by scanning electron microscope (SEM, JEOL JSM-6390A). Before measurements were taken, the sample was suspended in ethanol solution and dispersed in ultrasonic bath for 1 min. Then, the suspensions were added dropwise onto a copper tape for SEM analysis.

2.4. Reaction procedure

The catalytic performance of La_2O_3 catalysts doped by alkali and alkaline earth metals were tested via glycerol (GL) conversion with dimethyl carbonate (DMC) in a stainless-steel reactor (Yanzheng® YZPR-100). The thermocouple was built in a stainless-steel blind tube inside the reactor for the temperature control. The reaction mixture was stirred with a magnetic stirrer during the reaction.

The ratio 1:3 of GL and DMC was mostly claimed as optimal reactant ratio based on literature review [15,16,19,20,23–27], so in a typical experiment, 3.0 g of GL and 9.0 g of DMC were added into the reactor with 0.10 g of catalyst. After sealing the reactor, the mixture was continuously stirred and heated to a desired reaction temperature for a certain time. After this time was reached, the reactor was cooled down in an ice-water bath to stop the reaction. A certain amount of internal standard substance (ISTD), tetraethylene glycol, and DMF were added into the reaction mixture. Then the catalyst the catalyst was separated from the liquid phase in the centrifuge (SIGMA® 2-16P). The collected catalyst was retained and prepared for further recycling experiments. The obtained liquid phase was further analysed by gas chromatography (GC, Shimadzu GC-2010 plus), equipped with a flame ionization detector (FID) and a Stabilwax-MS (30 m × 0.25 mm) column. The qualitative analysis of the reaction products was carried via Shimadzu gas chromatography-mass spectra (GC–MS).

3. Results and discussion

In this section, the synthesis strategy of the wet impregnation method for doping alkali and alkaline earth metals on La_2O_3 catalysts is firstly illustrated in Section 3.1, then the catalyst characterisation obtained from the methods presented above for pristine La_2O_3 catalyst and La_2O_3 catalysts modified by 25 mol% alkali and alkaline earth metals are systematically discussed in Section 3.2. The catalytic performances of the pristine La_2O_3 and modified La_2O_3 catalysts in GL and DMC transesterification are then presented in Section 3.3, along with a discussion of the key characteristics which might affect the performance. The plausible mechanism was discussed based on modified La_2O_3 samples in Section 3.4. Finally, the optimal operating conditions for the transesterification of glycerol via doped La_2O_3 are shown in Section 3.5.

3.1. Synthesis strategy of La_2O_3 modified by alkali and alkaline earth metals

The wet impregnation method was used for modifying La_2O_3 catalyst with alkali and alkaline earth metals. The principle behind this method is discussed based on synthesising Na/La_2O_3 catalyst which is shown in Scheme 2. The synthesis procedure includes three main steps: impregnation, drying, and calcination. During the first step of impregnation, the pre-synthesised La_2O_3 powder is uniformly dispended in the $NaNO_3$ aqueous solution containing the Na^+, NO_3^-, H^+ and OH^- ions, and part of La_2O_3 phase could be transferred into $La(OH)_3$ and $La_2O_2CO_3$ phases during contact of water and CO_2 [28], and the reaction mechanisms are defined by Eq. (1) and Eq. (2) respectively. During the impregnation, Na^+ ions might diffuse into the pores of La_2O_3 and be adsorbed onto the porous surface, and Na^+ ions could also be adsorbed on the external surface of the support by forming the ion pair with its oxo/hydroxo-groups [29].

During the drying procedure, the precursor of Na^+ forms a homogenous distribution of the $Na_x(NO_3)_y(OH)_z$ crystals on the surface of the La_2O_3 (or on $La(OH)_3$ and $La_2O_2CO_3$) crystal phases which is illustrated in Eq. (3),. As the solvent is removed during the drying process, it can result in a redistribution of the modified metal phase on the support material [30]. The dopants inside the pores which have a smaller size can more easily migrate out to the external surface and contribute to the formation of the $Na_x(NO_3)_y(OH)_z$ crystals. In the calcination step, $Na_x(NO_3)_y(OH)_z$ starts to decompose to $NaNO_3$ at 100–200 °C, then $NaNO_3$ is converted into molten salt at around 308 °C [31], where the molten salt phase can increase the mobility of Na which can lead Na to enter the lattice of the support material. As described in Eq. (4), the molten $NaNO_3$ salt firstly starts decomposing to $NaNO_2$ at 380 °C [31], and then the formed $NaNO_2$ salt further decomposes to Na_2O at around 600 °C [32–34]. In the meantime, $La(OH)_3$ and $La_2O_2CO_3$ phases can start converting into La_2O_3 at 600 °C and complete the conversion at around 800 °C [35]. The formation of surface defects also occurs during the calcination step [35,36].

$$La_2O_{3(s)} + NaNO_{3(aq)} + H_2O \rightarrow La_2O_{3(s)} + Na^+{}_{(aq)} + NO_3^-(aq) + H^+{}_{(aq)} + OH^-{}_{(aq)} \quad (1)$$

$$La_2O_{3(s)} + H_2O + CO_2 \rightarrow La_2O_{3(s)} + La(OH)_{3(s)} + La_2O_2CO_{3(s)} \quad (2)$$

$$La_2O_{3(s)} + Na^+{}_{aq} + NO_3^- aq + H^+{}_{aq} + OH^-{}_{aq} \rightarrow Na_x(NO_3)_y(OH)_z \bullet La_2O_{3(s)} \quad (3)$$

$$Na_x(NO_3)_y(OH)_z \rightarrow NaNO_3 \rightarrow NaNO_2 + O_2 \rightarrow Na_2O + NO + NO_2,\ Na_x(NO_3)_y(OH)_z \bullet La_2O_{3(s)} \rightarrow (Na)La_2O_{3(s)} \quad (4)$$

The synthesis strategy for doping other alkali and alkaline earth metals – Li, K, Mg, Ca, Sr, and Ba – on La_2O_3 is similar to that for Na doping La_2O_3, but the decomposition temperatures of their nitrates to oxides are different to that of $NaNO_3$ which are summarised in Table S1.

3.2. Catalyst characterisation

3.2.1. Bulk and surface composition analysis

The bulk and surface composition of La_2O_3 samples are analysed by ICP-OES and XPS, and the results are listed in Table S2. The bulk composition of each element tested by ICP-OES is consistent with the

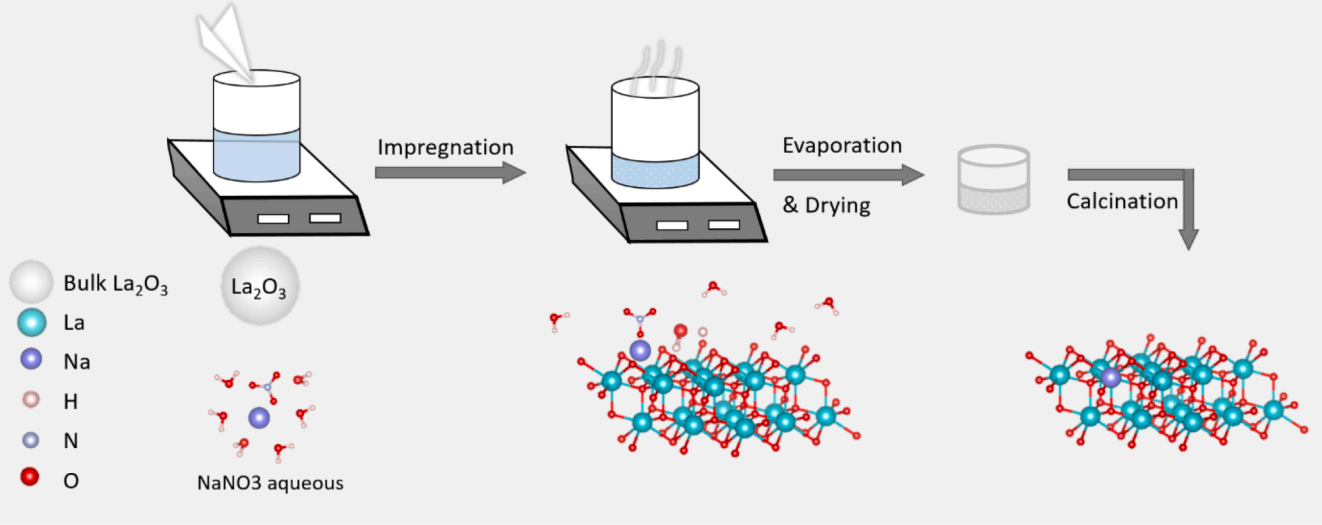

Scheme 2. Synthesis process of modifying La_2O_3 catalyst by Na.

designed composition where the amount of alkali and alkaline earth metals are around 25 mol% of La. While the surface compositions of Li and Na are around 68 % which are three times higher than their overall composition, that of Mg is about 48 % and two times higher than its bulk composition, and the surface composition for the other metals are similar to their bulk results. This result suggests that the majority of Li, Na and Mg are doped on the La_2O_3 surface, while K, Ca, Sr and Ba could form another phase along the bulk of La_2O_3. As illustrated in the synthesis strategy in Section 3.1, during the drying process, the dopants with smaller ionic radii more easily migrate out of the inner pores and adsorb on the surface. Zhang et al. [37] also found that the surface composition of Li and Na with smaller ionic radii are higher than K, due to Li and Na are more easily to migrate on the ZnO surface than K.

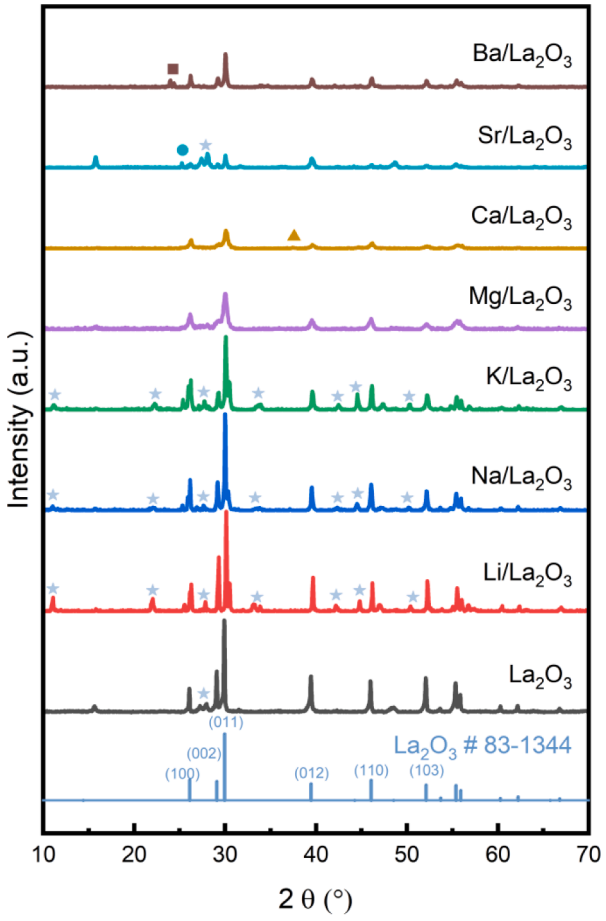

Fig. 1. XRD pattern of prepared La_2O_3 and La_2O_3 samples doped by alkali and alkaline earth metals, where the light blue stars represent $La_2O_2CO_3$ phase, the mustard yellow triangle represents CaO phase, the bright blue circle represents $SrCO_3$ phase, and the brown square represents $BaCO_3$ phase.

3.2.2. XRD analysis

The crystal structure of prepared La_2O_3 samples and the doping location of alkali and alkaline earth metals were studied via XRD analysis, and the results are shown in Fig. 1. The XRD patterns of pristine La_2O_3 and the modified La_2O_3 samples followed the hexagonal structure lanthanum oxide phase (*P*-3 m1, JCPDS 83–1344), and the main diffraction peaks of La_2O_3 are observed at $2\theta = 26.1°$, 29.1°, 29.9°, 39.5°, 46.0° and 52.1°, corresponding to the (1 0 0), (0 0 2), (0 1 1), (0 1 2), (1 1 0) and (1 0 3) crystal planes, respectively. The blue stars in Fig. 1 represent for the $La_2O_2CO_3$ phase (JCPDS 84–1963) which is inevitably formed when La_2O_3 sample is exposed to ambient atmospheric conditions [19,38]. In addition, no extra crystalline phases of alkali metal oxides were observed from their XRD patterns, therefore, the alkali metal could uniformly disperse on La_2O_3 surface [19,39,40]. Unlike surface doping, the bulk doping can influence the phase stability and crystal growth [40,41]. Diffraction peaks for alkaline earth metal doped La_2O_3 samples become much more weaken and broaden than that for alkali metal doped La_2O_3 samples, indicating the heavy doping of alkali earth metal inhibited the formation of La_2O_3 crystalline structure [41]. Nevertheless, the presence of CaO, $SrCO_3$, and $BaCO_3$ phase further confirmed that Ca, Sr, and Ba formed extra crystalline structure. These results suggest that most alkaline earth metals are incorporated in the bulk La_2O_3.

3.2.3. XPS analysis

X-ray photoelectron spectroscopy (XPS) analysis was used to clarify the electron environments for pristine and modified La_2O_3 samples. The XPS profiles for La 3d and O 1 s orbitals are shown in Fig. 2 and the corresponding binding energies of these orbitals are listed in Table S3. Due to spin–orbit coupling, the La 3d spectrum separated into two groups known as La $3d_{3/2}$ and La $3d_{5/2}$, respectively [19,42]. Each group can be further deconvoluted into one main peak (denoted as I), and two satellite peaks (denoted as II and III) [43,44]. The peaks of La $3d_{5/2}$ I for the pure La_2O_3 material are centred at 834.7 eV, and it is negatively shifted to between 834.2 eV and 834.4 eV for the La_2O_3 catalysts doped

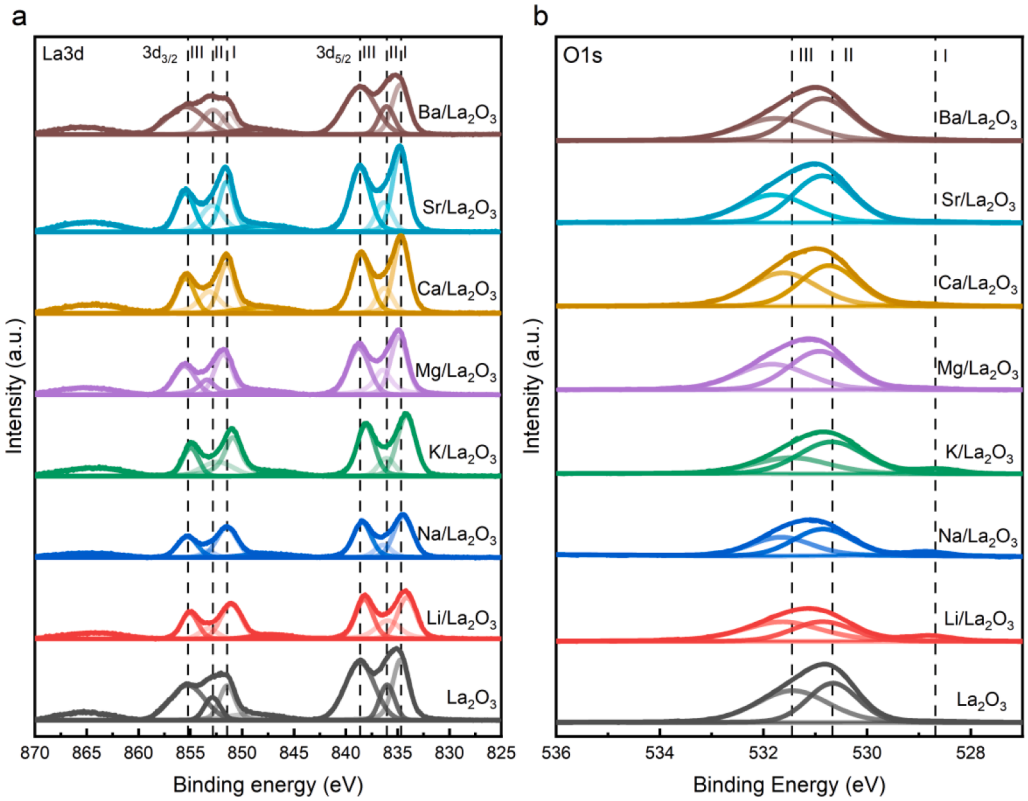

Fig. 2. XPS spectra of pristine La_2O_3 samples and La_2O_3 samples modified by alkali and alkaline earth metals: (a) La 3d, where peak I is the main peak, peak II and III are the satellite peaks; and (b) O 1 s, where peak I, II and III are represented for lattice O^{2-} (O_L), chemisorbed surface O^- (O_S) and weakly adsorbed OH^- and CO_3^{2-} (O_A) species, respectively.

by alkali metals, while no peak shifting was observed for the samples doped by alkaline earth metals. This result suggests that alkali metals donate electrons to La, which makes the La in alkali metal doped La_2O_3 catalysts be able to donate more electrons to reactants [39].

The peaks of O1s spectra are located at around 528.7 eV, 530.7 eV, and 531.4 eV, corresponding to the lattice O^{2-} (O_L), chemisorbed surface O^- (O_S) and weakly adsorbed OH^- and CO_3^{2-} (O_A) species, respectively [15,39,42,44]. The binding energy of O 1 s spectra are positively shifted towards the higher energy field for both La_2O_3 catalysts doped by alkali metals and alkaline earth metals, with the latter elements being shifted more. This result indicates that a larger amount of electrons transferred from O sites to alkaline earth metals than to alkali metals, which indicates that alkaline earth metals have a strong interaction with O in La_2O_3 [45,46]. This is also consistent with the XRD result discussed in the previous section that an extra phase of alkaline earth metal oxide was formed on the La_2O_3 surface.

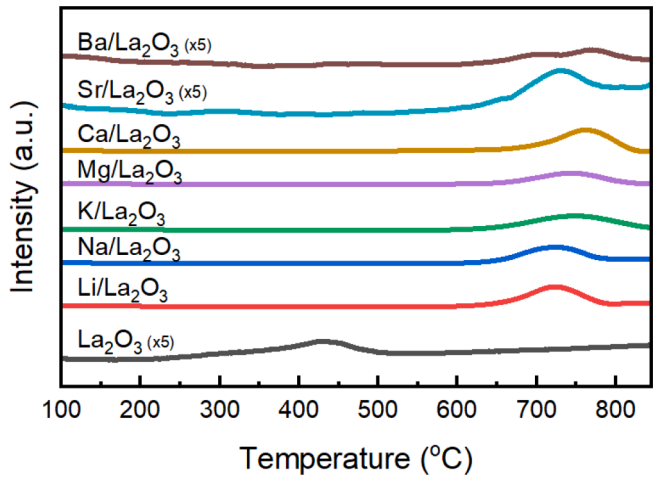

Fig. 3. CO_2 -TPD profiles of pure La_2O_3 and La_2O_3 catalysts modified by alkali and alkaline earth metals calcined at 600 °C.

3.2.4. CO_2 - TPD analysis

The surface basicity of La_2O_3 catalysts was measured by CO_2-TPD analysis and is shown in Fig. 3, and the corresponding densities of their basic sites are calculated and listed in Table S4. The CO_2 desorption peak for the pure La_2O_3 catalyst is centred at 400 °C – 500 °C, so the basic sites for pristine La_2O_3 sample can be denoted as strong basic site [19]. After doping alkali and alkaline earth metals on the La_2O_3 surface, the CO_2 desorption peaks shifted to a higher temperature field compared to that of pristine La_2O_3 sample and are located at 600 °C – 800 °C, in which the basic sites for the modified samples can be denoted as extra strong sites [19 47]. As a result, the basicity of the La_2O_3 sample became stronger with introducing alkali and alkaline earth metals. Additionally, alkali metal doped La_2O_3 samples contains 4.56–5.60 μmol/m^2 basic sites, higher than alkaline earth metal doped ones with 0.26–5.34 μmol/m^2 basic sites, which is consistent with the XPS results that the electrons around O in alkali metal doped La_2O_3 samples are more dense than those in alkaline earth metal doped La_2O_3 samples [47].

3.2.5. Physicochemical properties measurements

The average crystallite sizes of La_2O_3 and modified La_2O_3 were calculated via the Debyee-Scherrer equation, and the results are listed in Table S2, where the average crystal size of pure La_2O_3 is 68 nm, which is the largest of all the samples. The average crystal sizes of the alkali metal doped La_2O_3 samples were the next largest at about 42.2 nm-57.9 nm and the smallest were the alkaline earth metal doped La_2O_3 samples (at about 18 nm-34.3 nm). As a result, adding alkali and alkaline earth metal can hinder the growth of La_2O_3 crystal [30]. This is consistent

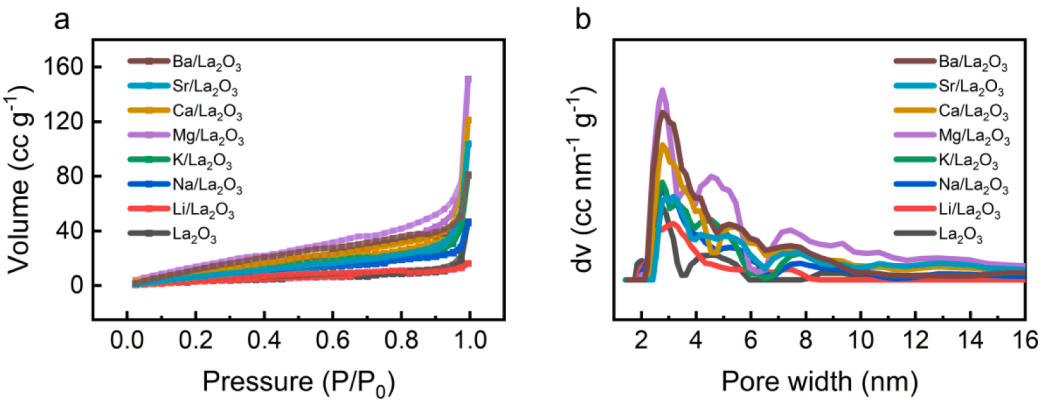

Fig. 4. (a) N_2 adsorption–desorption isotherms and (b) pore size distribution for pristine and modified La_2O_3 catalysts.

with their specific surface areas measured by N_2 isotherms which are shown in Fig. 4 a, and their specific surface areas, calculated by BET theory, are listed in Table S2. The surface areas of La_2O_3 samples doped by alkali metals are smaller than that of La_2O_3 samples doped by alkaline earth metals. The main pore size of all samples is distributed in the range of 2–4 nm, as shown in Fig. 4 b, while the pore width and total volume of modified La_2O_3 catalysts, especially in the range of 2–4 nm, became broader and higher than that of the pristine La_2O_3 catalysts. The surface morphologies of La_2O_3 and promoted La_2O_3 catalysts were individually determined by SEM analysis, and presented in Figure S1. The morphologies of the pure La_2O_3 sample and La_2O_3 samples doped by alkaline earth metals are similar and show a flake-like structure, while nanorod-like structures are shown in the La_2O_3 samples doped by alkali metals.

3.3. Catalytic performance

In this section, the catalytic performance of pristine La_2O_3 catalyst and modified La_2O_3 catalysts by alkali and alkaline earth metals are presented in Section 3.3.1, followed by a thorough discussion on the potential factors of the dopants and catalyst characteristics in improving the catalytic performance of La_2O_3.

3.3.1. Catalytic performance of pristine and modified La_2O_3 catalysts

The catalytic performance of the pristine La_2O_3 catalysts and the La_2O_3 catalysts modified by 25 mol% alkali and alkaline earth metals was examined in the transesterification of GL to GLC at 70 °C and 2 hrs and the results are presented in Fig. 5 a. The pristine La_2O_3 catalyst has barely any conversion of GL into GLC at 70 °C after 2 hrs, while doping alkali and alkaline earth metals on La_2O_3 catalysts significantly improved the catalytic performance of La_2O_3 catalyst in GL and DMC conversion. La_2O_3 catalysts doped by Li, Na and K achieved 48 %, 85 % and 40 % GL conversion, respectively, and the GL conversions for La_2O_3 catalysts doped by Mg, Ca, Sr and Ba were 13 %, 41 %, 21 % and 23 %, respectively. The GLC yield follows the similar trend as the GL conversion for alkali and alkaline earth metal doped La_2O_3 catalysts. Among all the modified La_2O_3 catalysts, Na doped La_2O_3 catalyst shows the best catalytic performance, and Ca doped La_2O_3 catalyst led to relatively higher GL conversion and GLC yield than the La_2O_3 catalysts doped by other alkaline earth metals. In addition, the alkali metal doped La_2O_3 catalysts showed relatively better catalytic performance than alkaline earth metal doped La_2O_3 catalysts.

To rule out the effect of molecular weight for doping metals, a fixed mass ratio, of alkali and alkaline earth metals were doped on La_2O_3 and tested in the GL transesterification, where the results are presented in Fig. 5b. The 3.5 wt% mass ratio of Na/La is the equivalent mass ratio to the 25 mol% of Na/La catalyst, and the equivalent molar ratios (eq. mol %) for other dopants are listed in Table 1. The catalytic performance of

Table 1
Equivalent molar ratio to the constant mass ratio (3.5 wt%); ionic radius and electronegativity of La, alkali metals and alkaline earth metals.

Catalyst	Mass Ratio and Its Equivalent Molar Ratio		Ionic Radius of Cation (Å)	Electronegativity (eV)
	wt%	eq. mol%		
La_2O_3	–	–	1.03 [19]	1.10
Li/ La_2O_3	3.5	83	0.76 [21]	0.98
Na/ La_2O_3	3.5	25	1.02 [21]	0.93
K/ La_2O_3	3.5	15	1.38 [21]	0.82
Mg/ La_2O_3	3.5	24	0.72 [48]	1.31
Ca/ La_2O_3	3.5	15	0.99 [48]	1.00
Sr/ La_2O_3	3.5	7	1.12 [48]	0.95
Ba/ La_2O_3	3.5	4	1.30 [48]	0.89

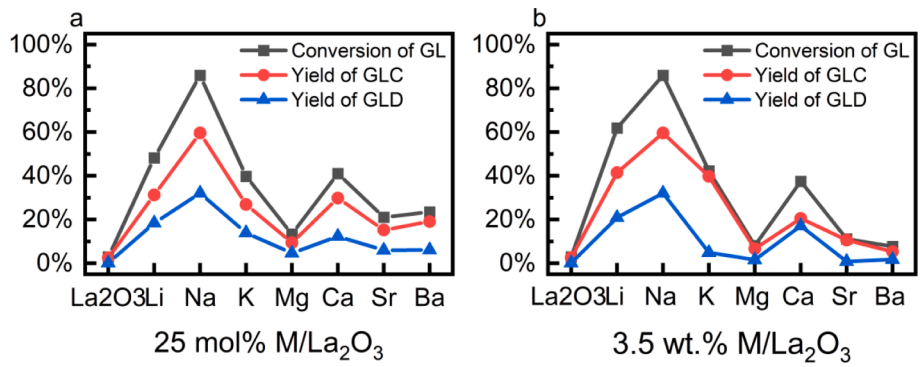

Fig. 5. The catalytic performance of La_2O_3 doped by alkali metal and alkaline earth metals, (a) with the fixed molar ratio of 25 mol%, (b) with the fixed mass ratio 3.5 wt%. (Reaction condition: DMC:GL = 3:1, 0.10 g catalyst, 70 °C and 2 hrs).

La_2O_3 based catalysts with the fixed mass ratio shows a similar trend as that for the catalysts with a fixed molecular ratio. As shown in Fig. 5 b, 3.5 wt% Na/La_2O_3 and 3.5 wt% Ca/La_2O_3 catalyst also achieved the highest glycerol conversion of 85 % and 37 %, respectively, among La_2O_3 catalysts doped by alkali metal and alkaline earth metal, and La_2O_3 catalysts doped by alkali metals showed better catalytic performance than the ones doped by alkaline earth metals. This result shows that the molecular weight of dopants is not the dominant factor that determines the ability of alkali and alkaline earth metals on improving catalytic performance of La_2O_3 catalyst.

3.3.2. *Promotion effects of alkali and alkaline earth metals*

The catalytic performance of a catalyst is determined by its properties which can be tuned by the dopant added. So, in this section, the correlation between the catalyst properties and the catalytic performance are discussed, and the dominant effects of the dopants on improving the catalytic performance of La_2O_3 catalyst are revealed.

3.3.2.1. Effect of ionic radius and valence state. Interestingly, the ionic radius of Na (1.02 Å) and Ca (0.99 Å), listed in Table 1, is similar to the cation radius of La (1.03 Å), and Na/La_2O_3 and Ca/La_2O_3 catalyst have showed the best GL conversion and GLC yield among the La_2O_3 catalysts modified by alkali metals and alkaline earth metal, respectively, so the similarity in their radius might be the dominant factor in affecting the dopant interaction with support material. Thus, a correlation between the ionic radius and catalytic performance was established and shown in Fig. 6.

For alkali metal promoted La_2O_3 samples, the ionic radius ratio of Na/La is 0.99 which indicates the radii of Na^+ and La^{3+} are very similar, and the ionic radius ratio of Li/La and K/La are 0.74 and 1.34, indicating the radius of Li^+ and K^+ relatively smaller or larger than that of La^{3+}, respectively. Interestingly, the GL conversion under La_2O_3 catalyst doped by Na, which has a similar ionic radius with La, is higher than that under La_2O_3 catalyst doped by metals with a dissimilar ionic radius with La, such as Li and K. This result indicates that the La_2O_3 catalyst doped by a dopant with a similar ionic radius to La can maximise the improvement of its catalytic performance in glycerol and DMC transesterification. The same trend was also found for the La_2O_3 catalysts doped by alkaline earth metals, with Ca having the most similar ionic radius to La, and having the highest GL conversion among the alkaline earth metals. Song et al. [7] and Kaur et al. [20] also claimed that ZnO and ZrO_4 catalyst doped by lithium showed better catalytic performance than those catalyst doped by other alkali metals because Li has a similar ionic radius (0.76 Å) to Zn (0.74 Å) and Zr (0.72 Å). Therefore, the similarity of ionic radius for the dopant to its support material can be considered as one of the determining factors in improving the catalytic performance of the catalyst. The potential reason might be when the ionic radius of the dopant is smaller or larger than the support material, it could cause a significant structure distortion around the dopant, which might affect the stability of the active sites, so when the ionic radius is similar to the support cation, the formed active sites is more stable which leads to the better catalytic performance. Moreover, when comparing the dopants in the same period, the catalysts doped by alkali metals are superior to the ones doped by the alkaline earth metal in GL and DMC reaction, indicating that the valence state of the dopant also affects the catalytic performance of modified La_2O_3 catalysts.

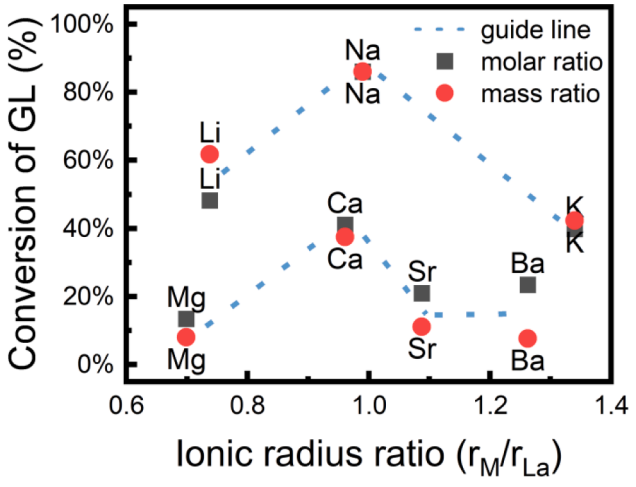

Fig. 6. Correlation between GL conversion and the ionic radius ratio of dopant and La, where the glycerol conversion was carried out at the same condition for each catalyst (Reaction condition: DMC:GL = 3:1, 0.10 g catalyst, 70 °C and 2 hrs).

3.3.2.2. Effect of surface concentration of dopants. The surface concentration of alkali and alkaline earth metals was tested via XPS, as stated in Section 3.2.1, and the surface concentration of Li, Na and Mg is higher than their overall concentration, where that of K, Ca, Sr, and Ba is similar to their overall concentration. It has been reported that surface doping might be better than bulk doping [40], but in this work, the surface concentration of the dopant did not show a proportional effect on the catalytic performance of modified La_2O_3 catalysts. For instance, the surface concentration of Li and Na is similar, but 25 mol% Na doped La_2O_3 catalyst achieved 85 % GL conversion, much better than 48 % GL conversion for 25 mol% Li doped La_2O_3 catalysts at the same reaction conditions. In addition, 25 mol% Mg/La_2O_3 catalyst achieved less GL conversion than 25 mol% Ca/La_2O_3 catalyst, although the surface concentration of Mg as about two times higher than that of Ca. Thus, the surface concentration is not the dominant factor for La_2O_3 catalysts doped by alkali and alkaline earth metals showing different catalytic ability in GL conversion.

3.3.2.3. Effect of the crystal structure. The diffraction peaks for La_2O_3 catalysts doped by alkaline earth metals from XRD analysis as shown in Fig. 1 are much broader and weaker than those for the pristine La_2O_3 catalysts and the ones doped by alkali metals, which agrees with the previous study [49,50]. The broader and weaker peaks could result from the formation of a non-crystalline phase, the aggregation of particles [51], or an incomplete La_2O_3 crystal phase. As illustrated in the synthesis strategy, given in Section 3.2.2, La_2O_3 can easily transfer to $La(OH)_3$ and $La_2O_2CO_3$ phases when it comes into contact with water or carbon dioxide in the atmosphere, so during the drying and calcination process, the $La(OH)_3$ and $La_2O_2CO_3$ gains are decomposed into La_2O_3 and rebuild the crystalline structure. Castro et al. [41] reported that alkaline earth metals, especially Mg and Ca, could prevent host material reforming from the calcination process. So a higher calcination temperature 800 °C was used to synthesise the modified La_2O_3 catalysts, and their XRD patterns, as shown in Figure S2, indicate a better crystalline structure of hexagonal lanthanum oxide was formed. Conversely, the catalytic performance for the samples calcined at 600 °C is better than that for the samples calcined at 800 °C (as shown in Figure S3), despite the crystal structures being well formed at 800 °C. In addition, the catalyst calcined at 800 °C achieved a similar trend as the ones calcined at 600 °C in GL and DMC conversion, where Na/La_2O_3 and Ca/La_2O_3 showed the best catalytic performance among the La_2O_3 catalysts doped by alkali metals and alkaline earth metals, respectively, and the alkali metal doped La_2O_3 catalysts showed relatively higher GL conversion than alkaline earth metals doped La_2O_3 catalysts. Thus, these results further suggest that the crystallisation degree for La_2O_3 catalysts doped by alkaline earth metals is not responsible for improving the catalytic performance.

3.3.2.4. Effect of the electronic environment. The full analysis of electronic states of La_2O_3 catalysts modified by alkali and alkaline earth metals is given in Section 3.2.3, where alkali metals as dopants on La_2O_3

catalysts can donate their electrons to La but alkaline earth metals showed little effect on the electronic environment of La. This might be due to the alkali metals having a lower electronegativity than alkaline earth metals [52], meaning alkali metals are more likely to donate their electrons than alkaline earth metals. This phenomenon has also been reported on alkaline earth metals doped on ZrO_2 [51] and Ni/La_2O_3 catalysts [53]. Additionally, alkali metals affect the electron distributions around O sites, while alkaline earth metals as dopants on La_2O_3 catalysts more strongly affect the electron distributions around O sites, which could be due to the extra phase of alkaline earth metal oxides formed [51]. This result is consistent with their catalytic performance where alkali metal doped La_2O_3 catalysts showed relatively better catalytic performance of alkaline earth metal doped La_2O_3 catalysts, which further reveals that the valence states of alkali and alkaline earth metals is one of dominant factors. However, for dopants within the same group, this cannot explain the trend in their catalytic performance.

3.3.2.5. Effect of the density of basic sites. The basic sites have been reported to be an important factor for a catalyst to achieve high GL conversion, so the correlation between basic site density and catalytic activity of alkali and alkaline earth metals doped La_2O_3 is presented in Fig. 7. The basic site density of La_2O_3 catalyst significantly increased after doping with alkali and alkaline earth metals as presented in Table S3, but the catalytic activities of La_2O_3 based catalysts are not proportional to the density of their surface basic sites. For instance, the basic site density of Na/La_2O_3 and Ca/La_2O_3 catalysts are very similar (5.60 μmol/m^2 and 5.34 μmol/m^2, respectively), but the GL conversion under Na/La_2O_3 catalysts is about 40 % higher than that under Ca/La_2O_3 catalyst. In addition, the basic site density of Li and K doped catalysts are also close to that of Na doped La_2O_3 catalyst, but Li and K modified La_2O_3 catalysts showed much lower GL conversion and GLC yield than Na/La_2O_3 catalyst. Therefore, these results imply that basic sites are important to the transesterification of GL and DMC, but it is not a determining factor.

3.4. Plausible mechanism

The plausible mechanism for the transesterification of GL and DMC on the La_2O_3 catalyst is proposed and shown in Fig. 8. The carbonyl group of DMC and the hydroxyl group of GL are activated on the La site and the O site, respectively [25]. Then the activated GL anion attacks the carbonyl carbon of activated DMC to form a 1-(o-methoxy-carbonyl) glycerol complex (denoted as intermediate 1) and one molar methanol. The intermediate 1 then further cyclise to GLC with another molar of methanol. The addition of alkali metals on La_2O_3 catalysts can form the

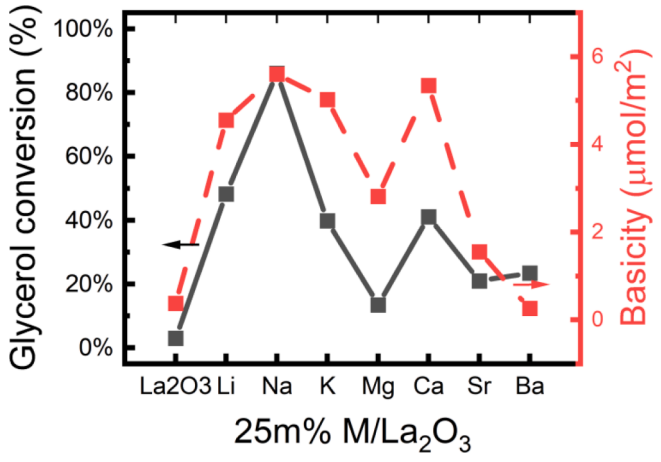

Fig. 7. Correlation between basic sites density and glycerol conversion, where the glycerol conversion was carried out at the same condition for each catalyst (Reaction condition: DMC:GL = 3:1, 0.10 g catalyst, 70 °C and 2 hrs).

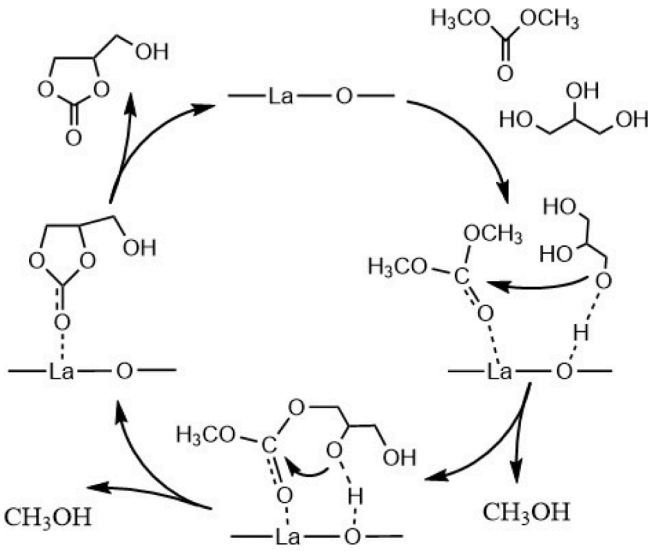

Fig. 8. Plausible mechanism of GL and DMC transesterification on Na/La_2O_3 catalyst.

M−La centre that help activate DMC and cyclise intermediate 1, which leads to higher GL conversion and GLC yield (as shown in Fig. 5 a) than the pristine La_2O_3 catalyst. The extra phase formed by adding alkaline earth metals can provide more active sites and benefit the catalytic reaction of GL and DMC. The better catalytic performance of La_2O_3 catalyst promoted by alkali metal than by alkaline earth metals can illustrate that M−La active centre could be more effective in reducing activation energy of the reaction than extra phase of alkaline earth metal oxide.

3.5. Optimisation of synthesis and reaction conditions

As La_2O_3 catalyst doped by 25 mol% Na achieved the highest GL conversion and GLC yield, Na/La_2O_3 catalyst was chosen for further investigation on the effect of dopant/support metal molar ratio, calcination temperature, catalyst dose, reaction temperature, reaction time and reusability. Each variable is considered independently using a standard set of conditions, and the best optimal condition for each variable is carried forward to the next variable analysis.

3.5.1. Effect of Na/La molar ratio

The impact of Na/La molar ratio for modified La_2O_3 (xNa/La_2O_3) was studied in the GL conversion to glycerol carbonate. The catalytic

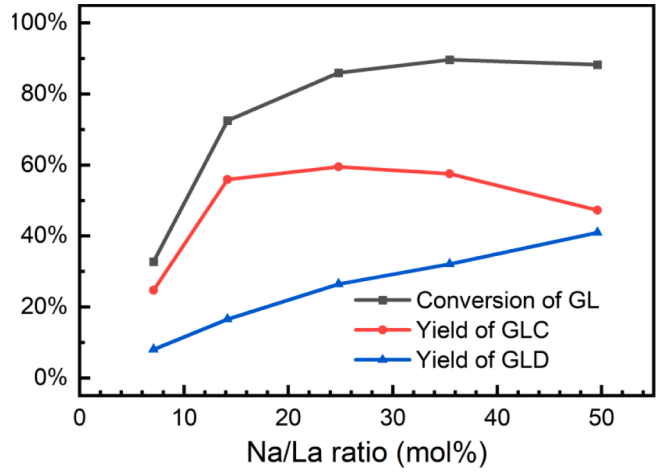

Fig. 9. Effect of Na doping amount on La_2O_3 (Reaction condition: DMC:GL = 3:1, 0.10 g catalyst, 70 °C, and 2 hrs).

activity of xNa/La_2O_3 calcined at 600 °C was studied under the reaction temperature of 70 °C for 2 hrs and the results are shown in Fig. 9. The result indicates the GL conversion was significantly increased from 32 % to 85 % with increasing the amount of Na from 7 mol% to 25 mol% doping on La_2O_3 catalysts, and the GLC yield was increased from 25 % to 59 % respectively. With increasing the amount of Na further to 50 mol% of La, GL conversion slightly increased to 89 %, but the GLC yield dropped to 47 % in which the yield of glycidol (GLD) increased from the decarbonation reaction of GLC. Therefore, it can be inferred that the GL conversion and GLC yield can be boosted with increasing amount of Na to 25 mol% of La_2O_3 catalyst due to an increase in the number of active sites, but further increasing the amount of Na benefits the generation of the by-product. Thus, to balance the high GL conversion and GLC yield, 25 mol% Na/La ratio was chosen as the optimal doping ratio, which are used for further optimisation.

3.5.2. *Effect of calcination temperatures*

To investigate the effect of calcination temperature on the catalyst activity, 25 mol% Na/La_2O_3 was calcined at various temperatures ranging from 400 °C to 800 °C, the obtained catalysts were tested in the GL and DMC conversion at 70 °C, and the reaction time was set for 2 h. The results are presented in Fig. 10 a. With the increase of calcination temperature from 400 °C to 600 °C, the GL conversion significantly increased from 5 % to 85 %, but then dropped from 85 % to 70 % with increasing the calcination temperature further to 800 °C. The crystalline structure of 25 mol% Na/La_2O_3 catalysts calcined at 400 °C to 800 °C was tested via XRD, and the result is presented in Fig. 10 b. When the 25 mol% Na/La_2O_3 catalyst was calcined at 400 °C and 500 °C, the catalyst was mainly in the $La_2O_2CO_3$ phase, which then gradually transferred to the La_2O_3 phase with increasing the calcination temperature, and La_2O_3 phase was the only phase presented at the Na/La_2O_3 catalyst calcined at 800 °C, which is consistent with the literature work [35]. In addition, the crystallinity of the catalysts increased with increasing the calcination temperature. These results indicate that $La_2O_3CO_3$ phase is not active in the conversion of GL into GLC. Increasing calcination temperature not only benefits to forming La_2O_3, but also promotes the $NaNO_3$ decomposition to Na_2O leading to better interaction with La_2O_3 catalyst. Although the La_2O_3 was also completely formed at 700 °C and 800 °C, the GL conversion and GLC yield are decreased with GLD yield increased which might be due to the aggregation of particles where Li et al. [19] reported a similar phenomenon of the decrease catalytic performance of Li/La_2O_3 catalyst calcined at 700 °C in GL and DMC conversion compared to the catalyst calcined at 600 °C. Thus, 25 mol% Na/La_2O_3 catalysts calcined at 600 °C were used for the further optimisation of reaction parameters.

3.5.3. *Effect of catalyst dose*

The amount of 25 mol% Na/La_2O_3 catalysts calcined at 600 °C was investigated in the range of 0.01 g to 0.20 g for 70 °C and 2-hour GL and DMC reactions. As shown in Fig. 11 a, with the amount of catalyst added from 0.01 g to 0.15 g, the production of GLC increases from 50 % to 60 % then drops to 40 % when further increasing the catalyst dose to 0.20 g, but the yield of by-product GLD also increased with the increase of catalyst dose. This result indicates that increasing the total number of active sites not only benefits the GL conversion to GLC, but also boosted the GLC decomposition to GLD. The catalyst performance peaks between 0.10 g and 0.15 g of catalyst, as the GLD yield is lower when 0.10 g 25 mol% Na/La_2O_3 catalyst was used, it seems to be more effective. Thus, 0.10 g of 25 mol% Na/La_2O_3 catalysts calcined at 600 °C was used for next optimisation of reaction temperature.

3.5.4. *Effect of reaction temperature*

The optimisation of the reaction temperature with 0.10 g of 25 mol% Na/La_2O_3 catalyst in GL and DMC conversion was carried out in the range of 50 °C – 90 °C for 2 hrs, and the result is presented in Fig. 11 b. The GL conversion significantly increases from 33 % to 96 % at a temperature increase from 50 °C to 80 °C. With temperature increasing further to 90 °C, the amount of glycerol converted is steady, but the yield of glycerol carbonate reduced. The maximum production of glycerol carbonate was 59 % when the reaction temperature was 70 °C. The glycerol transesterification to GLC is an endothermic reaction, therefore GL conversion increases with the reaction temperature increase [54]. However, the higher reaction temperature can drive GLC decomposed to GLD. Therefore, 70 °C was selected as the optimal reaction temperature.

3.5.5. *Effect of reaction time*

In the transesterification of glycerol and dimethyl carbonate, there is one primary product of glycerol carbonate and one by-product of glycidol. As shown in Fig. 11 c, with an increase in the reaction time from 0.5 hr to 4 hrs, the conversion of glycerol improved from 66 % to 95 %, and the yield of glycerol carbonate enhanced slightly from 58 % to 62 %. When the reaction time is beyond 2 hrs, the selectivity of GLC decreased and the amount of by-product GLD increased. So the optimal reaction time was selected as two hours.

3.5.6. *Reusability of the catalyst*

To investigate the reusability of the catalyst, the spent 25 mol% Na/La_2O_3 catalyst was recycled and reused in a fresh glycerol reaction operating at the optimal conditions (70 °C and 2 hrs), and the results are shown in Fig. 11 d. The catalyst activity slightly deceased after two cycles. The GL conversion dropped from 85 % to 71 % after the second cycle, and further dropped to 61 % after the fourth cycle. To reveal the reason of the deactivation, the following experiments were designed, and the results indicated that the catalyst decay is due to surface wearing which some active components lose in the solution as a fine powder because very high stirring speed (1000 rpm) was applied for the reaction system to ensure the catalyst well dispersing in the immiscible GL and DMC environment. In group A, to test whether the decay is caused in the

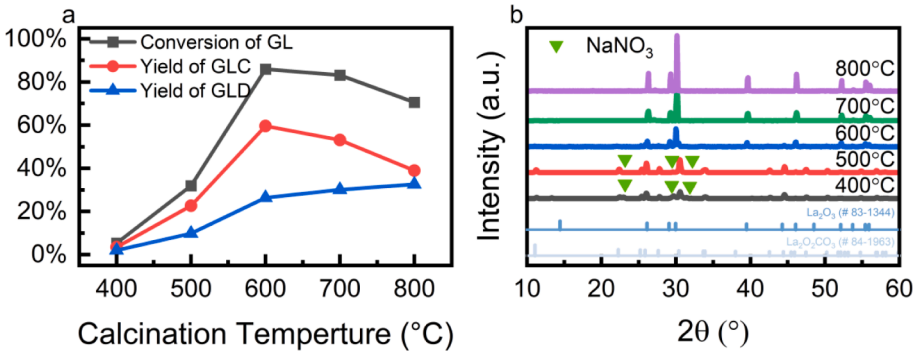

Fig. 10. (a) catalytic performance of 25 mol% Na/La_2O_3 catalysts calcined at 400 °C – 800 °C (Reaction condition: DMC:GL = 3:1, 0.10 g catalyst, 70 °C and 2 hrs); (b) XRD patterns for 25 mol% Na/La_2O_3 calcined at 400 °C – 800 °C.

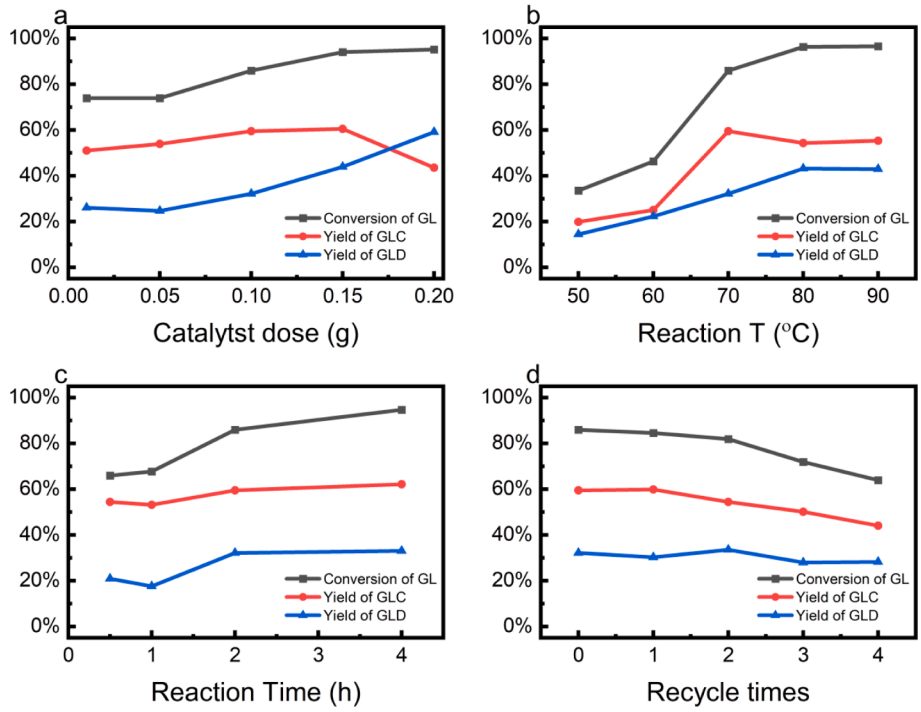

Fig. 11. Effect of reaction parameters: (a) catalyst dose; (b) reaction temperature; (c) reaction time; and (d) catalyst recycle.

Table 2
Deactivation test for Na/La_2O_3 catalyst.

Group	Catalyst treatment	GL conversion	GLC yield	GLC selectivity
A1	Pre-treated with Ethanol	84.99 %	68.42 %	95.76 %
A2	Pre-treated with DMF	83.71 %	67.34 %	95.69 %
B1	1 hr reaction with catalyst particles	67.80 %	53.17 %	95.34 %
B2	1 hr reaction after removing catalyst particle	79.59 %	60.38 %	94.59 %
C	Add $NaNO_3$ in reaction media	–	–	–

process of diluting reaction media or cleaning the residue reactants and products from the catalyst, the fresh Na/La_2O_3 catalyst was washed in ethanol (A1) and DMF (A2), respectively, at room temperature and dried completely at 110 °C in the oven before adding into the reactor. The glycerol conversion and GLC yield under pre-treated Na/La_2O_3 catalyst, shown in Table 2, are similar to that under fresh catalyst without treatment. Therefore, the solvents used in the regeneration process is not the reason causing the deactivation of the catalyst. In group B, the catalyst was separated from the reaction system via centrifuge after 1 hr reaction (B1), and after removing the catalyst particles the solution media continues the reaction for another 1 hr (B2). The results, listed in Table 2 for group B, show that the glycerol conversion and glycerol carbonate production increased after removing the catalyst particles from the reaction system, which revealed the some fine catalyst particles still remained in the solution and the deactivation of the catalyst likely resulted from wearing of active components from the catalyst surface. As the GL conversion continues after removing the La_2O_3 catalysts by centrifuge, one possible reason may be the leaching of Na ions from La_2O_3, and the leached Na promotes the reaction [7,19]. To clarify whether the deactivation is due to the leaching of Na ions from the doped La_2O_3, a certain amount of $NaNO_3$ was added in GL and DMC, but no products were detected from gas chromatograph as shown in group C. So the reaction cannot be conducted with only the presence of Na^+. As a result, the catalyst decay is not due to the leaching of Na^+ into reaction system. Thus, the catalyst deactivation is mainly due to the surface wearing rather than the regeneration process or leaching.

As the catalyst surface wearing is mainly caused by the friction between the magnetic stirrer and the bottom of the reactor, reducing the friction through increasing the volume of the solution and using mechanical agitator rather than a magnetic stirrer can be a potential solution to prevent the catalyst surface wearing. Moreover, using stronger support materials or coating the catalyst into stronger support materials, such as Al_2O_3 and ZrO_2, or applying advanced synthesis methods, such as sol–gel and precipitation, have been reported as effective way to prevent and reduce the catalyst decay from catalyst surface wearing [55].

4. Conclusions

Alkali and alkaline earth metal doped on La_2O_3 catalysts were successfully synthesised via a wet impregnation method, and their catalytic activities were tested in glycerol conversion to glycerol carbonate. Na was found to be the best dopant among the alkali and alkali earth metals for improving La_2O_3 catalytic performance, and 25 mol% Na doped La_2O_3 catalyst achieved highest GL conversion (85 %) and GLC yield (60 %) at 70 °C in a 2-hour reaction. La_2O_3 catalysts doped by alkali metals achieved relatively higher GL conversion and GLC yield than that doped by alkaline earth metals.

Ionic radius and valence state of dopants play significant roles in affecting the catalytic performance of La_2O_3 catalysts. In general, alkali metals were well dispersed on La_2O_3 surface, while alkaline earth metals were formed an extra phase and aggregated on La_2O_3 surface. The electron distribution around La on La_2O_3 surface was affected by doping alkali metal, while doping alkaline earth metal on La_2O_3 surface affected activity of O sites. The similarity of ionic radius between the dopant and La was found as one of the determining factors for improving La_2O_3 catalytic performance. The dopant with an ionic radius close to La led to a larger improvement in La_2O_3 catalytic activity than other dopants with a smaller or larger ionic radius, and the dopant with a lower valence state showed a better enhancement for La_2O_3 catalytic activity. The basic sites on La_2O_3 surface were found important to the

transesterification of GL and DMC, but the basic site density on modified La_2O_3 surface was not a determining factor for the catalytic performance of La_2O_3 catalysts. The findings about the effect of radius and charge of alkali and alkaline earth metals on La_2O_3 catalytic activity are expected to help to understand the promotional role of the dopant for designing more efficient and lower cost catalysts for glycerol value-added conversion to glycerol carbonate.

Declaration of Competing Interest

The authors declare that they have no known competing financial interests or personal relationships that could have appeared to influence the work reported in this paper.

Data availability

Data will be made available on request.

Acknowledgement

Thanks to the financial support from the UK research council EPSRC (EP/V041665/1). The authors appreciate Mr Fergus Dingwall from School of Engineering in The University of Edinburgh for all his technical support; Dr. Laetitia Pichevin and Dr. Nicola Cayzer from School of Geoscience in The University of Edinburgh for their kind help on ICP-OES and SEM analysis; and Dr. Gary Nichol from School of Chemistry in The University of Edinburgh for providing XRD facility and valuable advice.

Appendix A. Supplementary data

Supplementary data to this article can be found online at https://doi.org/10.1016/j.cej.2023.141486.

References

[1] G. Knothe, L.F. Razon, Biodiesel fuels, Prog. Energy Combust. Sci. 58 (2017) 36–59, https://doi.org/10.1016/j.pecs.2016.08.001.
[2] T.L. Alleman, R.L. McCormick, E.D. Christensen, G. Fioroni, K. Moriarty, J. Yanowitz, Biodiesel Handling and Use Guide (Fifth Edition), 2016. https://www.osti.gov/biblio/1347103.
[3] Y. Ji, Recent development of heterogeneous catalysis in the transesterification of glycerol to glycerol carbonate, Catalysts 9 (2019), https://doi.org/10.3390/catal9070581.
[4] M. Pagliaro, R. Ciriminna, H. Kimura, M. Rossi, C. Della Pina, From glycerol to value-added products, Angew. Chemie - Int. Ed. 46 (2007) 4434–4440, https://doi.org/10.1002/anie.200604694.
[5] M.O. Sonnati, S. Amigoni, E.P. Taffin De Givenchy, T. Darmanin, O. Choulet, F. Guittard, Glycerol carbonate as a versatile building block for tomorrow: Synthesis, reactivity, properties and applications, Green Chem. 15 (2013) 283–306, https://doi.org/10.1039/c2gc36525a.
[6] J.R. Ochoa-Gómez, O. Gómez-Jiménez-Aberasturi, C. Ramírez-López, M. Belsué, A brief review on industrial alternatives for the manufacturing of glycerol carbonate, a green chemical, Org. Process Res. Dev. 16 (2012) 389–399, https://doi.org/10.1021/op200369v.
[7] X. Song, Y. Wu, F. Cai, D. Pan, G. Xiao, High-efficiency and low-cost Li/ZnO catalysts for synthesis of glycerol carbonate from glycerol transesterification: The role of Li and ZnO interaction, Appl. Catal. A Gen. 532 (2017) 77–85, https://doi.org/10.1016/j.apcata.2016.12.019.
[8] J. Liu, Y. Li, H. Liu, D. He, Photo-thermal synergistically catalytic conversion of glycerol and carbon dioxide to glycerol carbonate over Au/$ZnWO_4$-ZnO catalysts, Appl. Catal. B Environ. 244 (2019) 836–843, https://doi.org/10.1016/j.apcatb.2018.12.018.
[9] P. Zhang, L. Liu, M. Fan, Y. Dong, P. Jiang, The value-added utilization of glycerol for the synthesis of glycerol carbonate catalyzed with a novel porous ZnO catalyst, RSC Adv. 6 (2016) 76223–76230, https://doi.org/10.1039/c6ra14288e.
[10] S. Ramesh, D.P. Debecker, Room temperature synthesis of glycerol carbonate catalyzed by spray dried sodium aluminate microspheres, Catal. Commun. 97 (2017) 102–105, https://doi.org/10.1016/j.catcom.2017.04.034.
[11] L. Zhang, S. Wang, Y. Guan, A. Zhang, S. Li, P. Hao, Synthesis of glycerol carbonate from glycerol and dimethyl carbonate catalyzed by calcined silicates, Appl. Catal. A Gen. 542 (2017) 174–181, https://doi.org/10.1016/j.apcata.2017.05.021.
[12] J.R. Ochoa-Gómez, O. Gómez-Jiménez-Aberasturi, B. Maestro-Madurga, A. Pesquera-Rodríguez, C. Ramírez-López, L. Lorenzo-Ibarreta, J. Torrecilla-Soria, M.C. Villarán-Velasco, Synthesis of glycerol carbonate from glycerol and dimethyl carbonate by transesterification: Catalyst screening and reaction optimization, Appl. Catal. A Gen. 366 (2009) 315–324, https://doi.org/10.1016/j.apcata.2009.07.020.
[13] S. Christy, A. Noschese, M. Lomelí-Rodriguez, N. Greeves, J.A. Lopez-Sanchez, Recent progress in the synthesis and applications of glycerol carbonate, Curr. Opin. Green Sustain. Chem. 14 (2018) 99–107, https://doi.org/10.1016/j.cogsc.2018.09.003.
[14] G. Pradhan, Y.C. Sharma, Green synthesis of glycerol carbonate by transesterification of bio glycerol with dimethyl carbonate over Mg/ZnO: A highly efficient heterogeneous catalyst, Fuel 284 (2021), 118966, https://doi.org/10.1016/j.fuel.2020.118966.
[15] P. Liu, M. Derchi, E.J.M. Hensen, Promotional effect of transition metal doping on the basicity and activity of calcined hydrotalcite catalysts for glycerol carbonate synthesis, Appl. Catal. B Environ. 144 (2014) 135–143, https://doi.org/10.1016/j.apcatb.2013.07.010.
[16] K. Hu, H. Wang, Y. Liu, C. Yang, KNO3/CaO as cost-effective heterogeneous catalyst for the synthesis of glycerol carbonate from glycerol and dimethyl carbonate, J. Ind. Eng. Chem. 28 (2015) 334–343, https://doi.org/10.1016/j.jiec.2015.03.012.
[17] Z. Bai, Y. Zheng, W. Han, Y. Ji, T. Yan, Y. Tang, G. Chen, Z. Zhang, Development of a trapezoidal MgO catalyst for highly-efficient transesterification of glycerol and dimethyl carbonate, CrstEngComm 20 (2018) 4090–4098, https://doi.org/10.1039/c8ce00808f.
[18] D.R. Lide, CRC Handbook of Chemistry and Physics, 89th Edition, Taylor & Francis, 2008 https://books.google.co.uk/books?id=KACWPwAACAAJ.
[19] Y. Li, J. Liu, D. He, Catalytic synthesis of glycerol carbonate from biomass-based glycerol and dimethyl carbonate over Li-La_2O_3 catalysts, Appl. Catal. A Gen. 564 (2018) 234–242, https://doi.org/10.1016/j.apcata.2018.07.032.
[20] A. Kaur, A. Ali, Lithium Zirconate as a Selective and Cost-Effective Mixed Metal Oxide Catalyst for Glycerol Carbonate Production, Ind. Eng. Chem. Res. 59 (2020) 2667–2679, https://doi.org/10.1021/acs.iecr.9b05747.
[21] Y. Sugiura, Y. Saito, T. Endo, Y. Makita, Effect of the Ionic Radius of Alkali Metal Ions on Octacalcium Phosphate Formation via Different Substitution Modes, Cryst. Growth Des. 19 (2019) 4162–4171, https://doi.org/10.1021/acs.cgd.9b00656.
[22] V.J. Ferreira, P. Tavares, J.L. Figueiredo, J.L. Faria, Effect of Mg, Ca, and Sr on CeO_2 based catalysts for the oxidative coupling of methane: Investigation on the oxygen species responsible for catalytic performance, Ind. Eng. Chem. Res. 51 (2012) 10535–10541, https://doi.org/10.1021/ie3001953.
[23] B. Das, K. Mohanty, Exploring the Promotional Effects of K, Sr, and Mg on the Catalytic Stability of Red Mud for the Synthesis of Glycerol Carbonate from Renewable Glycerol, Ind. Eng. Chem. Res. 58 (2019) 15803–15817, https://doi.org/10.1021/acs.iecr.9b00420.
[24] G.P. Deshmukh, G.D. Yadav, Tuneable transesterification of glycerol with dimethyl carbonate for synthesis of glycerol carbonate and glycidol on MnO_2 nanorods and efficacy of different polymorphs, Mol. Catal. 515 (2021), 111934, https://doi.org/10.1016/j.mcat.2021.111934.
[25] P. Devi, U. Das, A.K. Dalai, Production of glycerol carbonate using a novel Ti-SBA-15 catalyst, Chem. Eng. J. 346 (2018) 477–488, https://doi.org/10.1016/j.cej.2018.04.030.
[26] S.E. Kondawar, C.R. Patil, C.V. Rode, Tandem synthesis of glycidol via transesterification of glycerol with DMC over ba-mixed metal oxide catalysts, ACS Sustain. Chem. Eng. 5 (2017) 1763–1774, https://doi.org/10.1021/acssuschemeng.6b02520.
[27] D. Phadtare, S. Kondawar, A. Athawale, C. Rode, Crystalline $LaCoO_3$ perovskite as a novel catalyst for glycerol transesterification, Mol. Catal. 475 (2019), 110496, https://doi.org/10.1016/j.mcat.2019.110496.
[28] P. Fleming, R.A. Farrell, J.D. Holmes, M.A. Morris, The rapid formation of $La(OH)_3$ from La_2O_3 powders on exposureto water vapor, J. Am. Ceram. Soc. 93 (2010) 1187–1194, https://doi.org/10.1111/j.1551-2916.2009.03564.x.
[29] A. Lycourghiotis, Interfacial Chemistry, in: K.P. de Jong (Ed.), Synth. Solid Catal., 2009: pp. 13–31. https://doi.org/10.1002/9783527626854.ch2.
[30] P. Munnik, P.E. De Jongh, K.P. De Jong, Recent Developments in the Synthesis of Supported Catalysts, Chem. Rev. 115 (2015) 6687–6718, https://doi.org/10.1021/cr500486u.
[31] N.C. for B. Information, PubChem Compound Summary for CID 24268, Sodium Nitrate, (n.d.). https://pubchem.ncbi.nlm.nih.gov/compound/Sodium-Nitrate (accessed January 3, 2023).
[32] B.D. Bond, P.W.M. Jacobs, The thermal decomposition of sodium nitrate, J. Chem. Soc. A Inorganic, Phys. Theor. (1966) 1265–1268, https://doi.org/10.1039/J19660001265.
[33] K. Kawai, T. Fukuda, Y. Nakano, K. Takeshita, Thermal decomposition analysis of simulated high-level liquid waste in cold-cap, EPJ Nucl. Sci. Technol. 2 (2016) 44, https://doi.org/10.1051/epjn/2016038.
[34] K.H. Stern, High Temperature Properties and Decomposition of Inorganic Salts Part 3, Nitrates and Nitrites, J. Phys. Chem. Ref. Data. 1 (1972) 747–772, https://doi.org/10.1063/1.3253104.
[35] Y.H. Hou, W.C. Han, W.S. Xia, H.L. Wan, Structure sensitivity of $La_2O_2CO_3$ catalysts in the oxidative coupling of methane, ACS Catal. 5 (2015) 1663–1674, https://doi.org/10.1021/cs501733r.
[36] G. Li, C. Peng, C. Zhang, Z. Xu, M. Shang, D. Yang, X. Kang, W. Wang, C. Li, Z. Cheng, J. Lin, Eu^{3+}/Tb^{3+}-Doped $La_2O_2CO_3$/La_2O_3 nano/microcrystals with multiform morphologies: Facile synthesis, growth mechanism, and luminescence properties, Inorg. Chem. 49 (2010) 10522–10535, https://doi.org/10.1021/ic101541q.
[37] M. Zhang, Y.u. Liu, S. Wang, D. Zhang, P. Li, M. Wang, P. Hu, HuijinTao, HuijinTao, Effects of different alkali metal ions on morphology and photocatalysis

properties of ZnO crystals via hydrothermal method, Mater. Res. Innov. 23 (5) (2019) 247–252.
[38] J. Song, Y. Sun, R. Ba, S. Huang, Y. Zhao, J. Zhang, Y. Sun, Y. Zhu, Monodisperse Sr-La_2O_3 hybrid nanofibers for oxidative coupling of methane to synthesize C2 hydrocarbons, Nanoscale 7 (2015) 2260–2264, https://doi.org/10.1039/c4nr06660j.
[39] K. Sutthiumporn, S. Kawi, Promotional effect of alkaline earth over Ni-La_2O_3 catalyst for CO_2 reforming of CH_4: Role of surface oxygen species on H_2 production and carbon suppression, Int. J. Hydrogen Energy. 36 (2011) 14435–14446, https://doi.org/10.1016/j.ijhydene.2011.08.022.
[40] S.-M. Chang, W.-S. Liu, Surface doping is more beneficial than bulk doping to the photocatalytic activity of vanadium-doped TiO_2, Appl. Catal. B Environ. 101 (3–4) (2011) 333–342.
[41] C.S. Castro, C. Ferreti, J.I. Di Cosimo, J.M. Assaf, Support influence on the basicity promotion of lithium-based mixed oxides for transesterification reaction, Fuel 103 (2013) 632–638, https://doi.org/10.1016/j.fuel.2012.06.072.
[42] D. Briggs, X-ray photoelectron spectroscopy (XPS), Handb. Adhes. Second Ed. (2005) 621–622. https://doi.org/10.1002/0470014229.ch22.
[43] M.F. Sunding, K. Hadidi, S. Diplas, O.M. Løvvik, T.E. Norby, A.E. Gunnæs, XPS characterisation of in situ treated lanthanum oxide and hydroxide using tailored charge referencing and peak fitting procedures, J. Electron Spectros. Relat. Phenomena. 184 (2011) 399–409, https://doi.org/10.1016/j.elspec.2011.04.002.
[44] J.P.H. Li, X. Zhou, Y. Pang, L. Zhu, E.I. Vovk, L. Cong, A.P. Van Bavel, S. Li, Y. Yang, Understanding of binding energy calibration in XPS of lanthanum oxide by: In situ treatment, Phys. Chem. Chem. Phys. 21 (2019) 22351–22358, https://doi.org/10.1039/c9cp04187g.
[45] R. Bekkari, L. Laânab, B. Jaber, Effect of the bivalent dopant ionic radius, electronegativity and concentration on the physical properties of the sol–gel-derived ZnO thin films, J. Mater. Sci. Mater. Electron. 31 (2020) 15129–15139, https://doi.org/10.1007/s10854-020-04078-z.
[46] S. Shao, K. Wang, J.B. Love, J. Yu, S. Du, Z. Yue, X. Fan, Water promoted photocatalytic C_β-O bonds hydrogenolysis in lignin model compounds and lignin biomass conversion to aromatic monomers, Chem. Eng. J. 435 (2022), 134980, https://doi.org/10.1016/j.cej.2022.134980.
[47] M.A.A. Aziz, A.A. Jalil, S. Wongsakulphasatch, D.V.N. Vo, Understanding the role of surface basic sites of catalysts in CO_2 activation in dry reforming of methane: A short review, Catal Sci. Technol. 10 (2020) 35–45, https://doi.org/10.1039/c9cy01519a.
[48] V.R. Choudhary, S.A.R. Mulla, V.H. Rane, Surface basicity and acidity of alkaline earth-promoted La_2O_3 catalysts and their performance in oxidative coupling of methane, J. Chem. Technol. Biotechnol. 72 (1998) 125–130, https://doi.org/10.1002/(SICI)1097-4660(199806)72:2<125::AID-JCTB880>3.0.CO;2-3.
[49] T.W. Elkins, S.J. Roberts, H.E. Hagelin-Weaver, Effects of alkali and alkaline-earth metal dopants on magnesium oxide supported rare-earth oxide catalysts in the oxidative coupling of methane, Appl. Catal. A Gen. 528 (2016) 175–190, https://doi.org/10.1016/j.apcata.2016.09.011.
[50] H.V. Lee, J.C. Juan, Y.H. Taufiq-Yap, Preparation and application of binary acid-base CaO-La_2O_3 catalyst for biodiesel production, Renew. Energy. 74 (2015) 124–132, https://doi.org/10.1016/j.renene.2014.07.017.
[51] C. Zhong, X. Guo, D. Mao, S. Wang, G. Wu, G. Lu, Effects of alkaline-earth oxides on the performance of a CuO-ZrO_2 catalyst for methanol synthesis via CO_2 hydrogenation, RSC Adv. 5 (2015) 52958–52965, https://doi.org/10.1039/c5ra06508a.
[52] K. Wang, J. Fu, Y. Zheng, Insights into photocatalytic CO_2 reduction on C_3N_4: Strategy of simultaneous B, K co-doping and enhancement by N vacancies, Appl. Catal. B Environ. 254 (2019) 270–282, https://doi.org/10.1016/j.apcatb.2019.05.002.
[53] Y.H. Ahmad, A.T. Mohamed, A. Kumar, S.Y. Al-Qaradawi, Solution combustion synthesis of Ni/La_2O_3 for dry reforming of methane: Tuning the basicity via alkali and alkaline earth metal oxide promoters, RSC Adv. 11 (2021) 33734–33743, https://doi.org/10.1039/d1ra05511a.
[54] J. Li, T. Wang, Chemical equilibrium of glycerol carbonate synthesis from glycerol, J. Chem. Thermodyn. 43 (2011) 731–736, https://doi.org/10.1016/j.jct.2010.12.013.
[55] M.D. Argyle, C.H. Bartholomew, Heterogeneous catalyst deactivation and regeneration: A review, Catalysts 5 (2015) 145–269, https://doi.org/10.3390/catal5010145.